Title
Investigation of the transduction mechanism of infrared detection in Melanophila acuminata: photo-thermal–mechanical hypothesis

Journal
Comparative Biochemistry and Physiology Part A Molecular & Integrative Physiology, 132(2)

ISSN
1095-6433

Authors
Hammer, DX
Davé, D
Milner, TE
et al.

Publication Date
2002-06-01

DOI
10.1016/s1095-6433(02)00036-3

ELSEVIER

Comparative Biochemistry and Physiology Part A 132 (2002) 381–392

CBP

www.elsevier.com/locate/cbpa

Investigation of the transduction mechanism of infrared detection in *Melanophila acuminata*: photo-thermal–mechanical hypothesis

D.X. Hammer*, D. Davé, T.E. Milner, B. Choi, H.G. Rylander III, A.J. Welch

Department of Electrical Engineering, University of Texas, Austin, TX 78712, USA

Received 29 August 2001; received in revised form 19 January 2002; accepted 22 January 2002

Abstract

Differential phase optical low coherence reflectometry (OLCR) was used to detect sub-wavelength displacements in the infrared-sensitive thoracic pit organ of *Melanophila acuminata* (Coleoptera: Buprestidae) upon absorption of infrared radiation at 3.39 μm. The displacement had more complex morphology but similar amplitude (~100 nm at 1 W cm^{-2}) when compared to the displacement measured from the exocuticle in an alternate region on the beetle's body. In addition, a simplified finite difference model was developed to predict the temperature distribution and resultant thermal expansion in the pit organ tissue. The experimental and model results were interpreted to help clarify the mechanism by which the sensilla in the pit organ convert infrared radiation to neural signals. The results of this paper are discussed in relation to the photo-thermal–mechanical transduction hypothesis. This is the first experimental examination of the transduction mechanism in *Melanophila acuminata*.

Keywords: *Melanophila acuminata*; Differential phase optical low coherence reflectometry; Interferometry; Transduction mechanism; Photo-thermal–mechanical; Infrared receptor

1. Introduction

Several recent reports have described electrophysiological experiments performed on the infrared (IR) sensitive beetle *Melanophila acuminata* (Coleoptera: Buprestidae) (Schmitz and Bleckmann, 1998; Hammer et al., 2001a). The beetle is able to detect IR radiation of wavelengths between approximately 2.5 and 5 μm, in the atmospheric window which corresponds to the blackbody radiation peak emitted by a typical forest fire (Schmitz et al., 2000; Hammer et al., 2001b). The IR sensitivity allows the beetles to navigate to an area of weakened and defenseless trees in which to bury their eggs prior to competing species (Linsley, 1943). Using electron microscopy, investigators have described the ultrastructure of the pit organ responsible for IR detection (Vondran et al., 1995; Schmitz and Bleckmann, 1997). The bilateral thoracic pit organ consists of 50–100 sensilla that are each composed of a spherule in which the dendritic tip of a single neuron is embedded.

Investigators have hypothesized that the mechanism of transduction from infrared radiation to neural signal takes place, in part, by mechanical means (Vondran et al., 1995; Schmitz and Bleckmann, 1998). According to this photo-thermal–mechanical hypothesis, infrared energy is absorbed by the spherule, which produces a thermal expansion. The expansion causes mechanical compression of the dendritic tip that elicits a neural response (Fig. 1). Examination of the material properties and spectral sensitivity of the organ has provided evidence of correlation between the sen-

*Corresponding author. Physical Sciences Inc., 20 New England Business Center, Andover, MA 01810, USA. Tel.: +1-978-738-8224; fax: +1-978-687-7211.

E-mail address: hammer@psicorp.com (D.X. Hammer), dpdave@mail.utexas.edu (D. Davé), milner@ece.utexas.edu (T.E. Milner), bchoi@laser.bli.uci.edu (B. Choi), rylander@mail.utexas.edu (H.G. Rylander III), welch@mail.utexas.edu (A.J. Welch).

1095-6433/02/$ - see front matter
PII: S1095-6433(02)00036-3

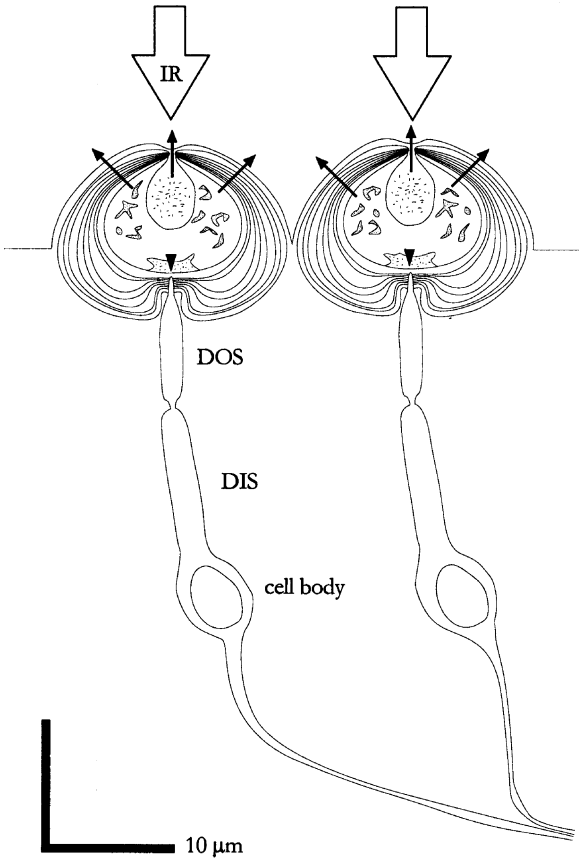

Fig. 1. Speculated transduction mechanism in the IR pit organ. Absorption of IR energy causes thermal expansion of the spherule (arrows) and subsequent compression of the dendritic tip (arrowheads). DIS, dendritic inner segment; DOS, dendritic outer segment.

silla tissue absorption and the wavelengths to which the beetle selectively responds (Hammer et al., 2001b). Vondran et al. (1995) provide a solid argument, based upon observations of electron microscope images, for the conversion to neural signals by thermo-mechanical deformation of the dendritic tip. They rule out chemical photoreception, due to the absence of any rhabdom-like structure in the dendritic outer segment, a basic feature of insect photoreceptors. Moreover, the fact that the absorption peaks of all known photopigments lie below 700 nm and the unlikelihood that low energy quanta of infrared radiation can trigger a molecular response in pigment further suggest that the pit organ does not function by chemical photoreception. They rule out a purely thermoreceptive mechanism due to differences in the dendrite from typical insect thermoreceptors. For example, the dendritic tips of thermoreceptors are lamellated or branched and do not contain tubular bodies or make direct contact with the cuticular apparatus of the sensillum. This morphology is in contrast to that observed in the IR sensillum of *Melanophila acuminata.* Finally, Vondran et al. list several similarities between the IR receptor and insect hair mechanoreceptors (sensillum trichodeum). These include the eccentric insertion of the tip into the cuticular apparatus (i.e. spherule in the IR sensillum), the presence of a tubular body in the dendritic tip, and the attendant wax gland.

Moreover, the existence of 'suppressed systems' in the posterior wall of the pit with features common to both suggest a possible descent of the IR receptor from a hair mechanoreceptor. Although differences exist between the IR receptor and the insect hair mechanoreceptor, most notably the shape of the tip: circular in the mechanoreceptor and laterally compressed in the IR receptor, these differences are thought to be related to the form of mechanical stimulus presented, i.e. expansion of a spherule in the IR receptor and deflection of a seta in the mechanoreceptor. Thus, electron microscopy observations have provided strong indirect evidence that the sensilla in the IR pit organ function in part by mechanical means.

Despite the strength of the morphological evidence, to date no experiments have been reported that seek to validate the photo-thermal–mechanical transduction hypothesis. Vondran et al. (1995) concluded the postulation of the photo-thermal–mechanical hypothesis discussed in the previous paragraph with a suggestion to measure the spherule expansion with a laser interferometer. The experiments described in this paper were designed with Vondran's suggestion in mind. The goal of this research is not only to begin the process of experimentation whereby the complete transduction pathways (including the molecular transduction mechanisms) will eventually be discovered, but also to determine which methodology is best suited for the task. The authors make no pretense that this experiment will definitively prove a particular transduction hypothesis. For example, the transduction mechanism of infrared detection in pit vipers and boids is still debated among herpetologists despite availability of experimental data collected over the last 50 years (Bullock and Cowles, 1952; Moiseenkova et al., 2001). In this paper an interferometric method used to detect a

minute displacement in the pit organ tissue that occurs upon absorption of infrared radiation is discussed. The results described are the first experimental examination of the transduction mechanism in *Melanophila acuminata.*

An interferometric method, differential phase optical low-coherence reflectometry (Davé and Milner, 2000), was used to measure small movements in the IR pit organ that occur when the spherule absorbs infrared light. In this technique, the phase difference between interference signals from two orthogonal polarization channels is recorded. Phase measurement allows detection of sub-wavelength changes in optical path length, thus improving resolution over detection of intensity changes alone. Differential phase measurement allows rejection of common-mode phase noise due to environmental perturbations. Complete isolation and decorrelation of the two polarization channels eliminates the contribution to the interference signal of cross-coupled back-reflected light from the sample. In addition to OLCR measurements, a simple finite difference model was developed to predict the temperature distribution and resultant thermal expansion in the spherule.

2. Materials and methods

2.1. Fiber-based optical low coherence reflectometer

The fiber-based differential phase OLCR system used to measure a small movement in the pit organ of the beetle upon excitation with IR radiation is shown in Fig. 2a. The OLCR system was designed to measure the differential phase between two equal-amplitude, orthogonally-polarized, decorrelated channels of a fiber Michelson interferometer (Davé and Milner, 2000). The partially polarized broadband light centered at 1.3 μm ($\Delta\lambda = 60$ nm) from the source (optical semiconductor amplifier, AFC Technologies Inc., model BBS 1310BTS) is linearly polarized (the polarizer P is external to the fiber). The polarized light input into a length of birefringent fiber separates into linear polarized light along the fast and slow axes of the fiber. A Lyot depolarizer is used to ensure that equal amplitudes are coupled into each of the two orthogonal polarization states of the single-mode birefringent fiber and that the two channels are decorrelated. A 45° splice between two segments of birefringent fiber will split the amplitude of each axis equally into the fast and slow axes of the second fiber. Temporal delay introduced in the birefringent fiber between polarization modes far exceeds the coherence time (coherence length/velocity of light) of the source. If the length of the second segment of birefringent fiber is at least twice that of the first segment, the two channels will be completely decorrelated. Although incident linearly polarized light that is reflected back from a highly scattering sample object may depolarize and couple into both modes of the birefringent fiber, interference fringes in each channel will only be formed between light of the same polarization in the reference and sample paths. Light from a semiconductor diode laser ($\lambda = 0.633$ μm) is coupled into the fiber interferometer with a wavelength division multiplexor (Gould Fiber-Optics, Inc.) and used as an aiming beam. The 0° splices in the input arm couple light between different types of fiber (e.g. standard single-mode and birefringent fiber) or between lengths of fiber with different core diameter. The source light is split into reference and sample arms with a polarization-maintaining coupler (Canadian Instrumentation, Inc.). A lithium niobate ($LiNbO_3$) waveguide (JDS Uniphase, Inc.) modulates the phase of the slow axis of the reference arm at a fixed frequency (50 kHz, controlled by external function generator, Stanford Research Systems Inc., model DS345).

The 45° splice prior to the phase modulator assures that both polarization channels are modulated. Only the slow axis from the fiber is coupled into the phase modulator. In this application, only a single channel of the phase modulator is used. A grating pair is used in the reference arm to compensate for waveguide and material dispersion. The 90° splice in the sample arm is necessary to ensure the optical path lengths in both polarization channels are matched and coherence functions are superposed.

Orthogonal polarization components from the reference and sample arms interfere in the coupler. These interference signals are spatially separated with a 20° Wollaston prism and focused onto two low-noise, 125-MHz infrared indium gallium arsenide (InGaAs) photoreceivers (New Focus Inc., model 1811). The signals are amplified and bandpass filtered (10–300 kHz) with a dual-channel differential amplifier (Preample Inc., model 1822 PR2) and recorded via a 50 MS s^{-1} (for two channels), 12-bit data acquisition (DAQ) card

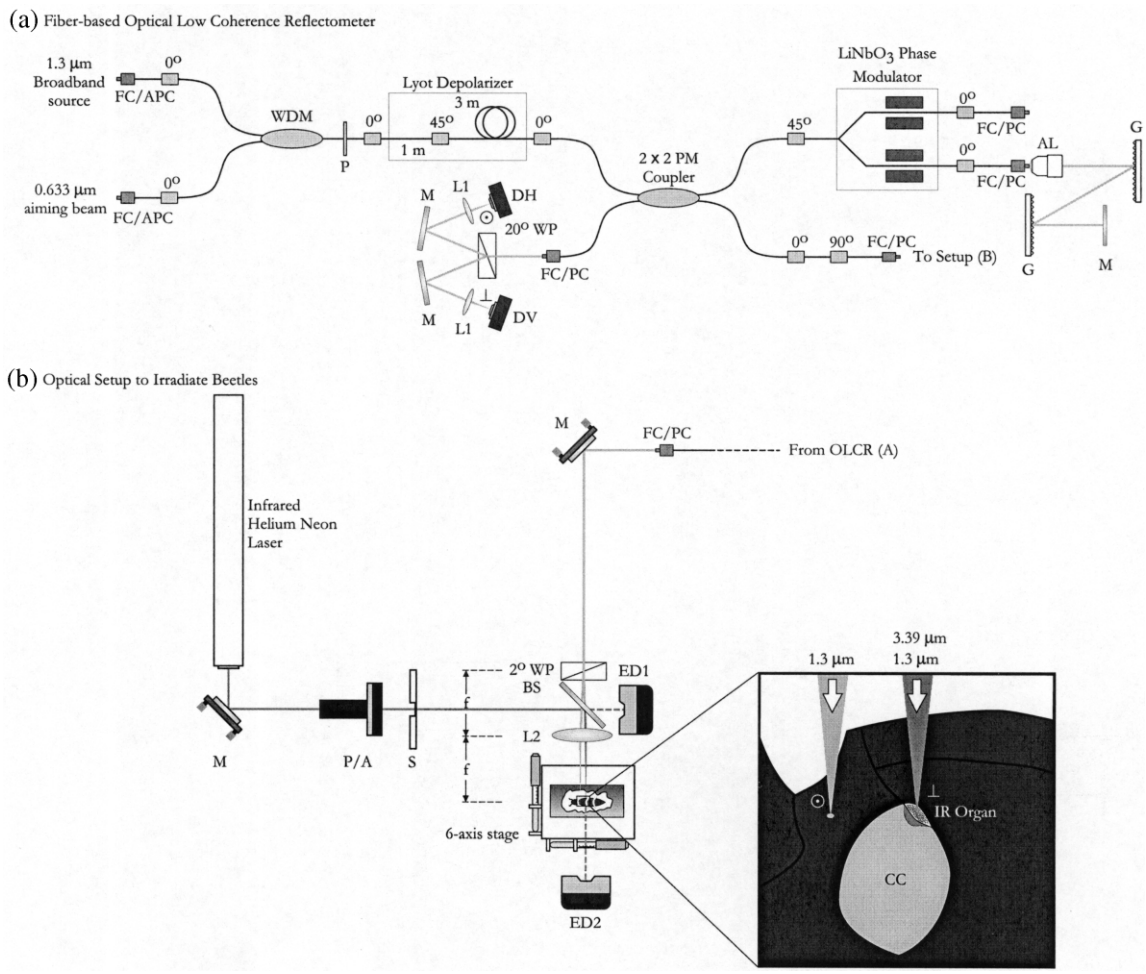

Fig. 2. (a) Fiber-based optical low coherence reflectometer and (b) optical setup used to irradiate beetles. Inset of (b) illustrates position of beams on the thorax of the beetle. FC, fiber connector; WDM, wavelength division multiplexor; PM, polarization-maintained coupler; AL, 11-mm focal length aspheric lens; G, grating; DH–DV, horizontal and vertical detectors; M, mirror; P/A, polarizer/attenuator; BS, BaF_2 broad-band infrared beam-splitter; ED1-2, power meters; S, shutter; WP, Wollaston prism; L1, detector lens; L2, 50-mm focal length CaF_2 lens; CC, coxal cavity.

(Gage Inc., model #CS12100) installed in a personal computer.

2.2. Optical setup

Light from the sample arm of the OLCR, was spatially separated into two polarization components with a 2° Wollaston prism and focused with a 50-mm focal length CaF_2 lens onto the exocuticle of the *Melanophila* beetle (see inset of Fig. 2b). The Wollaston prism and beetle were placed at the back and front focal planes of the CaF_2 lens, respectively, to give two parallel beams focused onto the beetle. One of the beams was focused onto the infrared pit organ while one was focused onto the adjacent exocuticle. Care was taken to find a location on the beetle that resulted in minimal path length difference between the beams. Small path length differences between the two channels were compensated by translation of the Wollaston prism in the sample arm perpendicular to the optical axis, which increased the optical path length in one of the two channels. The pit organ was excited with 3.39-μm radiation from a helium–neon laser (Research Electro-Optics Inc.). The helium–neon laser also emits light at 1.15 μm, which was used to align the beam collinear to the OLCR beam that was directed onto the infrared pit organ. Near- and mid-infrared light

beams were made collinear with the use of a BaF_2 broadband infrared beamsplitter. The ratio of power reflected to that transmitted through the beamsplitter (ED2/ED1) was used to correct the power recorded on ED1 (Molectron Inc., EPM2000 power meter and PM-3 head) to obtain an accurate measure of the power incident on the beetle. The incident power level was controlled with a polarizer/attenuator (II–IV Inc., model PAZ-20-AC-4) and external infrared filters. The beam radius (213 μm) of the IR helium–neon laser at the pit organ (in front of the focus) was measured with the knife-edge technique (ISO, 1999). The focused beam radius of the OLCR beam was not measured but since its wavelength is three times smaller and the beetle was positioned near the focus for this wavelength (1.3 μm), it is estimated to be approximately 35 μm, roughly the size of 3–4 sensilla. A miniature scale marked the beetle location for knife-edge measurement and a surgical microscope aided in alignment of the OLCR aiming beam onto the infrared pit organ. The sample path collimator that directed the OLCR beam onto the beetle was placed on a mechanical stage that could be translated along the optical axis to vary position of the coherence function relative to the pit. Although interference fringes could be detected from light that had backscattered from positions well into the pit organ, the coherence function was adjusted to measure the differential phase of light reflected from the region closest to the surface of the pit organ.

Two million data points recorded at a sampling rate of 5 MS s^{-1} (400 ms) were acquired into the buffer of the DAQ card. The acquisition was triggered on the DAQ card by a signal from the shutter (Vincent Associates Inc., Uniblitz model T132 shutter driver and model VS14 shutter). For constant duration IR irradiation ($\lambda = 3.39$ μm), the shutter pre-delay and exposure duration were both set to 100 ms, while the power was varied. For constant IR power measurements, the exposure duration was varied from 0.3 to 100 ms. The live beetle with unperturbed pit organ (i.e. in its natural state with wax layer) was fixed in dental glue and prepared as described previously (Hammer et al., 2001a).

Relative changes in the pit organ surface position due to IR irradiation were measured with OLCR in three configurations: two experimental and one control. The control configuration was with one OLCR beam aligned on the pit organ, one aligned on the exocuticle, and the 3.39-μm wavelength excitation beam blocked. This configuration measured any baseline phase change between OLCR channels. The first experimental configuration, depicted in the inset of Fig. 2b, was with one OLCR beam aligned collinear to the excitation laser on the IR pit organ and one OLCR beam aligned on the adjacent exocuticle. Provided the control group did not show a significant phase change, the phase change in this configuration can be attributed entirely to the displacement of the pit organ upon absorption of infrared radiation. The second experimental configuration was with the excitation laser placed on the exocuticle of the thorax collinear to one OLCR beam, and the other OLCR beam placed on an adjacent portion of the thorax. Since the thermal and material properties of many different tissue types allow for an expansion upon absorption of infrared radiation, comparison of the two experimental configurations yielded information about the specific role of the pit organ in infrared transduction. Irradiation of the thorax in the second configuration was only performed at higher irradiance values ($\sim$1.5 W cm^{-2}).

2.3. Data processing

The interference fringe intensity signals in both channels were centered around a 50-kHz carrier frequency and sampled at 5 MS s^{-1} then digitally filtered with a third-order Butterworth bandpass filter from 45 to 55 kHz. A forward–reverse filter was used to assure zero phase distortion. An example of a portion of the unfiltered and filtered signals is shown in Fig. 3. The instantaneous phase was extracted from the filtered signals with a Hilbert transform, unwrapped, and the two channels compared. The change in path length Δl is related to the phase change ϕ by,

$$\Delta l = \frac{\phi \lambda}{4\pi} \quad (1)$$

where λ is the center wavelength of the OLCR source light. The phase sensitivity of the system was 0.05 radians ($\sim$5 nm). Since the organ displacement occurred on a relatively slow time scale (milliseconds) compared to the sampling frequency, the data were decimated (without averaging) subsequent to phase difference calculation and prior to further analysis.

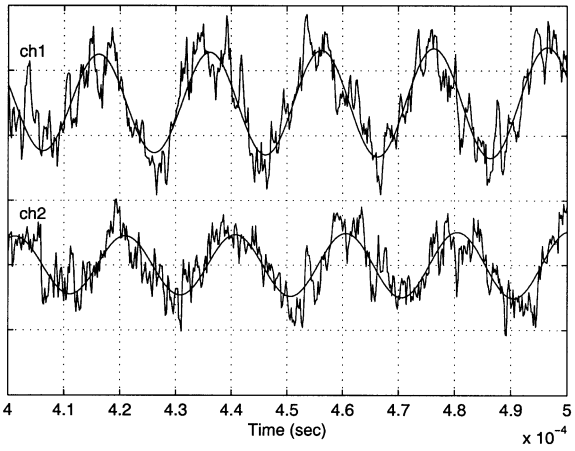

Fig. 3. Example of unfiltered and filtered fringes from two channels of the optical low coherence reflectometer.

The differential phase OLCR system can detect relative displacement (change in path length between two sites) that is correlated to a specific event, in this case the opening and closing of the shutter that controls IR exposure. Since the phase change is relative, nothing can be said of the direction of displacement unless the phase change is bipolar. For this reason, signal averaging could not be used for absolute quantification of the response magnitude unless the waveforms were first rectified. Rectification was not used because it distorts the response shape and hence corrupts any qualitative information from the signals. Therefore, data processing software was written to measure the amplitude of maximum displacement either in the positive or negative direction. The quantification of any other waveform variable (e.g. latency and duration) was difficult due to phase drift and other noise inherent to the OLCR system; however, qualitative trends were found.

2.4. Finite difference modeling

A one-dimensional implicit finite difference model was used to predict the temperature distribution in the pit organ. Although the model may be an over-simplification of the complex mechanisms involved in infrared absorption and subsequent displacement, simulation results serve as a starting point for comparison to displacements measured with OLCR. More complex models that include a realistic geometry for the pit organ can be formulated using the results of our simple numerical model.

Our simplified model utilized existing finite difference code developed by the authors to investigate laser photothermal effects (Choi et al., 2000; Choi and Welch, 2001; Incropera and DeWitt, 1996). Briefly, finite difference models are numerical solutions to the heat transfer equation for discretized time and space. The material (i.e. tissue) is divided into nodes, and the transfer of heat by conduction or convection at each node is calculated according to the conservation of energy for incremental time steps. An explicit model calculates node temperature according to the temperature of adjacent nodes for previous time steps. An implicit model calculates node temperature based on the temperature of adjacent nodes for current time steps. The choice of time steps in the explicit model must satisfy stability requirements, whereas the implicit model is inherently stable. The temperature as a function of tissue depth and time are two typical model results.

For the temperature rise from absorption of infrared radiation in the beetle pit organ, several assumptions and simplifications were made. A one-dimensional model was used because the beam radius of the excitation laser ($\lambda = 3.39$ μm) was large (213 μm) compared to both penetration depth in pit organ tissue (15 μm) and radius of the OLCR laser (35 μm). The model treated the pit organ as a semi-infinite slab of homogeneous tissue. Since wax covers the pit organ in its natural state, the model did not include convection at the boundary. Absorption but not scattering of incident infrared radiation was included. Therefore, Beer's law was assumed to govern the distribution of radiation with depth,

$$\phi(z) = E_0 \exp(-\mu_a z) \quad (2)$$

where $\phi(z)$ is the fluence rate (J s^{-1} cm^{-2}), μ_a is the absorption coefficient (cm^{-1}) and E_0 is the incident irradiance. The model source term was,

$$S(z) = \mu_a \phi(z). \quad (3)$$

In the finite difference model, the laser radiation was deposited according to Beer's Law in incremental amounts during each time step. Once the finite difference model was used to calculate the temperature distribution as a function of time and tissue depth, the displacement (Δz) was found from the temperature increase (ΔT) at each node,

$$\Delta z = \alpha z \Delta T \quad (4)$$

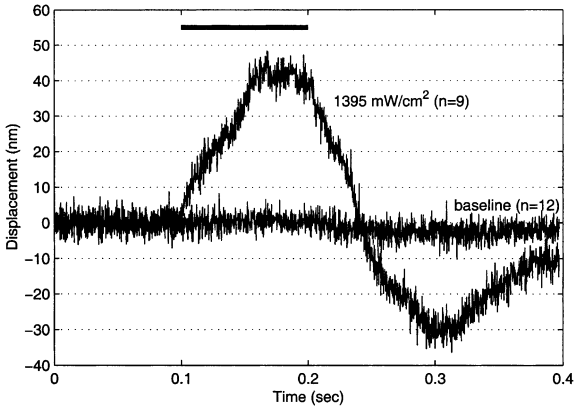

Fig. 4. Average displacement of the pit organ for high incident irradiance (1395 mW cm^{-2}) and with the infrared laser blocked (baseline). The displacement at high irradiance has a characteristic bipolar shape. Exposure duration (100 ms) is indicated by a bar above both waveforms. Number of waveforms averaged (n) is given.

where α is the coefficient of linear expansion and z is the initial node thickness. The displacement of the entire pit organ was found by summation of the individual node displacements over a tissue depth of 100 μm, which represents approximately six optical depths at 3.39 μm.

In the extreme case of no heat conduction, the total temperature rise due to absorption of infrared radiation is,

$$\Delta T(z,\tau)=\frac{\mu_a E_0 \tau}{\rho c}\exp(-\mu_a z) \quad (5)$$

where τ is the exposure duration, ρ is the material density (g cm^{-3}) and c is the specific heat (J g K^{-1}). Eq. (5) is the maximum temperature rise possible if the absorbed energy is converted to an increase in tissue temperature.

For the model, the absorption coefficient at 3.39 μm ($\mu_a=660$ cm^{-1}) and the conductivity ($k=8\times10^{-3}$ W cm^{-1} K^{-1}) measured previously were used (Hammer, 2001). For comparison, the absorption coefficient at 3.39 μm and the conductivity of water are 721 cm^{-1} and 6×10^{-3} W cm^{-1} K^{-1}, respectively (Querry et al., 1991; Pearce and Thomsen, 2000). Values for the density-specific heat product ($\rho\cdot c=1.5$ J cm^{-3} K^{-1}) and the linear coefficient of expansion ($\alpha=4\times10^{-4}$ K^{-1}) in a range typical for tissues ($\rho\cdot c=1$–6 J cm^{-3} K^{-1} and $\alpha=1$–6×10^{-4} K^{-1}) were used (Duck, 1990). The values selected provided the best fit to the experimental data.

3. Results

3.1. Pit organ and exocuticle displacement

Throughout the course of a particular experiment, the IR laser was blocked and a control waveform was acquired. Fig. 4 shows a comparison between the average displacement of the pit organ for high incident irradiance and the displacement of the pit organ when the IR laser was blocked. The latter waveform illustrates displacement unrelated to IR absorption by the pit organ.

The displacement of the pit organ as a function of irradiance for constant exposure duration is illustrated in Figs. 5 and 6. An unambiguous response correlated to the shutter trigger was found for irradiances down to approximately 200 mW cm^{-2}. For irradiances up to approximately 50 mW cm^{-2}, the displacement was equivalent to that of the control group. For irradiances between 50 and 200 mW cm^{-2}, identification of a response was difficult. Fig. 5 shows examples of single response waveforms for a range of incident irradiances. Fig. 6 shows the displacement as a function of irradiance for all the data collected from the beetles. As expected higher irradiances yielded larger displacements.

The displacement of the pit organ as a function of exposure duration for constant irradiance (1384 mW cm^{-2}) is illustrated in Figs. 7 and 8. An unambiguous response was recorded for durations

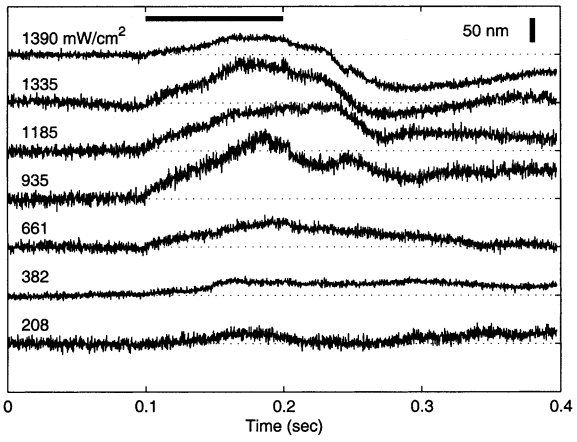

Fig. 5. Displacement of the pit organ for a range of incident irradiances. The morphology, amplitude, latency, and duration of displacement all depend upon irradiance. Irradiance is indicated above each waveform and exposure duration (100 ms) is indicated by a bar. Waveforms are offset by 100 nm.

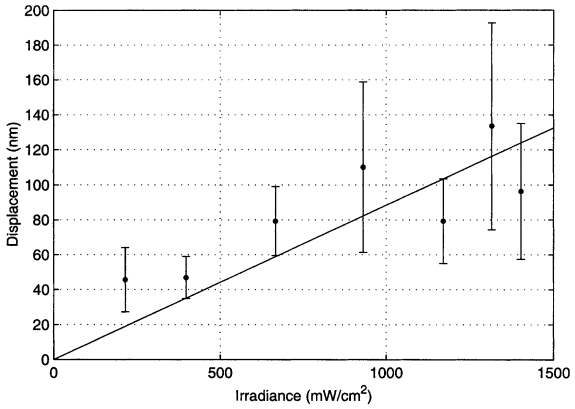

Fig. 6. Displacement of the pit organ as a function of incident irradiance. Error bars are the standard deviation of each set. The solid line is the displacement calculated from the finite difference model.

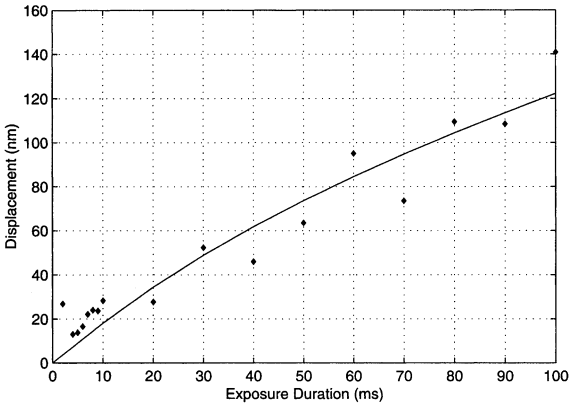

Fig. 8. Displacement of the pit organ of one beetle as a function of exposure duration at constant irradiance (1384 mW cm^{-2}). The solid line is the displacement calculated from the finite difference model.

down to 2 ms. Below 2 ms, the response was equivalent to the control group. Fig. 7 shows examples of single response waveforms for a range of exposure durations. Fig. 8 shows the displacement as a function of exposure duration for all the data collected from one beetle. As expected, longer durations yielded larger displacements.

The results of the second experimental configuration, which measured the displacement of exocuticle tissue on the thorax in a region away from the IR pit organ, is shown in Fig. 9. In this figure, the displacement for a single exposure at 1415-mW cm^{-2} irradiance and 100-ms duration is shown.

3.2. Finite difference model results

Figs. 6 and 8 show the displacement calculated from the finite difference model as a function of irradiance and exposure duration. Fig. 9 shows the temporal profile of the displacement. Fig. 10 shows temperature distribution at several times during and after a 100-ms pulse with an irradiance of 1 W cm^{-2}. The predicted displacement at this irradiance and pulse duration for a tissue thickness of 100 μm was 88 nm, of which 30 nm (34%) was

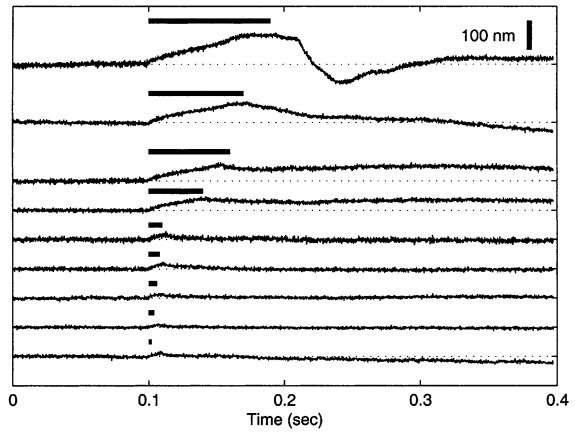

Fig. 7. Displacement of the pit organ for a range of exposure durations at constant irradiance (1384 mW cm^{-2}). The morphology, amplitude, and duration of displacement all depend upon duration. Exposure duration is indicated above each waveform by a bar. Waveforms are offset by 100 or 200 nm.

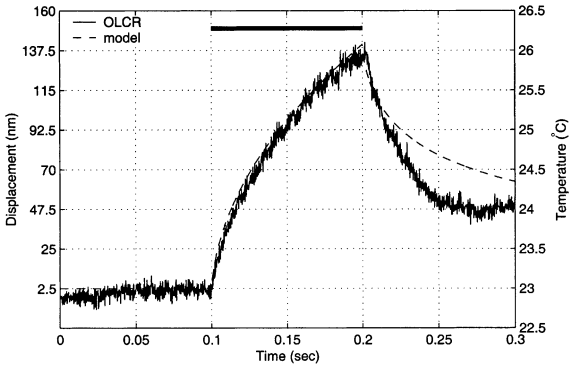

Fig. 9. Displacement of the exocuticle on the thorax (near pit organ) upon absorption of infrared radiation (left axis). The dashed line indicates surface temperature increase (right axis) over the exposure duration calculated from the finite difference model. Irradiance = 1415 mW cm^{-2}.

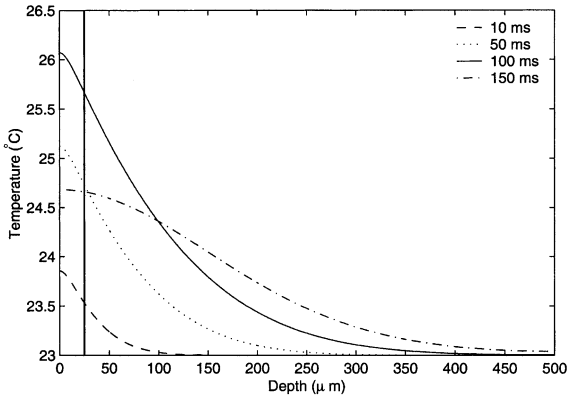

Fig. 10. Temperature of the pit organ as a function of tissue depth calculated from the finite difference model at several times (in milliseconds) during and after the laser exposure. Incident irradiance and exposure duration were 1 W cm^{-2} and 100 ms, respectively. The approximate extent of the spherule of sensilla (25 μm) is illustrated with a vertical line.

from the region that contained the spherule of the sensilla (25 μm).

4. Discussion

The sub-wavelength displacement measured by interferometric means is the first experimental investigation of the mechanism by which the pit organ of the beetle *Melanophila acuminata* converts infrared radiation to neural signals. The interrogation of the organ was entirely optical, and thus completely non-invasive. Although a measurable displacement of the pit organ surface was detected, an equivalent amplitude displacement was measured when the exocuticle on the thorax adjacent to the pit organ was irradiated. Thus, the expansion upon absorption of infrared radiation is not a unique response of the IR pit organ tissue in *Melanophila* beetles. There were, however, significant differences between the displacement recorded from the exocuticle and that recorded from the pit organ. The displacement recorded from the pit organ was often bipolar, especially at high irradiances and long exposure durations (see Figs. 5 and 7). This indicates that the pit organ moves in a complex manner that may include expansion, contraction, or lateral displacement. In contrast, the displacement of the exocuticle is similar in shape to the characteristic curve for a change in tissue temperature. In a typical temperature curve, if the pulse duration is short compared to the thermal relaxation time, a linear increase in temperature will be observed during the exposure duration. If the pulse duration is long enough to allow heat to be conducted away from the exposed tissue, as is the case for Fig. 9, an asymptotic increase in temperature during exposure duration will take place. In either case, when the shutter closes, a decay described by the error function occurs as the tissue is cooled.

Therefore, the results of this study are not definitive proof of a photo-thermal–mechanical mechanism and must be viewed, together with the electron microscopy (see Section 1), as additional evidence that may support that transduction mechanism hypothesis. The results also illustrate the limitation in interpretation of this implementation of differential-phase OLCR for the measurement of one-dimensional motion in biological tissue. The most direct evidence of mechanoreception requires more complex measurements that may include three-dimensional interferometric mapping of the spherule motion or biochemical analysis of channel pores in the dendritic tip of the primary neuron.

Fig. 9 also illustrates a novel application of differential-phase optical low coherence reflectometry in the configuration of Fig. 2. If a tissue is irradiated with an infrared laser to cause a temperature increase while the tissue is simultaneously probed with OLCR, a non-invasive characterization of tissue thermal properties can be accomplished. This application of differential-phase OLCR has great potential but requires significant further development and investigation.

While the irradiance values may initially seem quite high when compared to thermal sensors in other animals, the response range can be understood if the following points are considered. First, the detection threshold has been established in previous reports to be approximately 5–15 mW cm^{-2} (Schmitz and Bleckmann, 1998; Hammer et al., 2001a). Second, although the saturation value has not been definitively established, previous measurements suggest it lies within the range of 0.3–1 W cm^{-2} (Schmitz et al., 2000; Hammer et al., 2001b). This range is consistent with the data shown in Fig. 6, which shows an increase in displacement up to approximately 0.5–1 W cm^{-2} after which the displacement levels off. Last, in terms of a physiologically significant range, it must be kept in mind that the sensors detect radiant energy from forest fires. In a previous paper, it was calculated that the beetles should be able to

detect medium sized forest fires (10 ha, 700 °C) up to a distance of ~1 km using the threshold range above (Hammer et al., 2001a). At 100 m, the emittance exposed to the beetle will be closer to 1 W cm^{-2}. Since the ultimate function of the IR information to the beetle is not presently known, care must be made when comparing the characteristics of this sensor to other (especially temperature) sensors in insects and other animals. If the organ is used in close proximity (e.g. for safety purposes) rather than to detect forest fires from a great distance, a large dynamic range and high saturation level may be more important than high sensitivity.

The phase noise in the average waveforms of Fig. 4 and the individual waveforms of Figs. 5, 7 and 9 can be attributed to a number of factors. As alluded to in Section 2.1, any translational motion of the beetle along the optical axis will result in an equal shift of the interference fringes in both channels and will not be observed in the displacement waveforms because the OLCR technique employs differential phase detection (i.e. common-mode noise rejection). However, any movement of one part of the beetle with respect to the pit organ will result in a phase difference between channels. This type of displacement was usually observed on a slower time scale (i.e. at a lower frequency) and manifested as a slow phase drift. The phase noise was broad-band and thus could not be further digitally filtered. The phase noise ultimately determines the minimum resolvable change in displacement. In the ideal case, with a highly-reflective, optically-flat mirror in the sample arm of the OLCR system, the minimum resolvable displacement change was approximately 5 nm. In our experiments, the waveforms in Figs. 5 and 7 illustrate a minimum resolvable differential displacement of approximately 25 nm. This may explain why a distinguishable response was not seen below 200 mW cm^{-2}.

Figs. 5 and 7 show typical displacement signals for a range of incident powers and exposure durations, respectively. Both sets show a change in morphology, amplitude and duration. If the bipolar response seen at high irradiances is accurate, the response can be interpreted to mean that the spherule contracted to a volume smaller than its original volume after the shutter closed. However, since displacement in only a single dimension is measured, a complex change in sphere shape or possibly lateral translation of the spherule without a concomitant volumetric reduction is possible. Another feature of the displacement curves is the monotonic increase during the time the shutter is open. Since it was shown that receptor polarization elicits a phasic ON response (action potentials) from the primary neuron (Hammer et al., 2001a), this result may initially seem surprising. However, those electrophysiological experiments have shown that the firing of action potentials was predicated only on the polarization of the generator potential past a certain threshold. The generator potential continued to decrease to a minimum during the exposure in a manner similar to the displacement. An OFF response was also observed in the generator potential at high irradiances (unpublished observations).

Other qualitative observations of the displacement waveforms include a decrease in response duration with a decrease in power and exposure duration and an increase in latency (i.e. time from stimulus to response) with a decrease in power. The latency did not appear to change with exposure duration. Again, all of these observations are similar to those found for the generator potential. Thus, a correlation may exist between the displacement of a sensillum and the generator potential of the primary neuron.

The data in Fig. 8 show good agreement between measured and model displacement as a function of exposure duration. There is also fairly good agreement between model and experimental data in Fig. 6 despite large standard deviations, with perhaps a slight underestimation of the displacement by the model for irradiances less than 1 W cm^{-2} and a possible saturation of displacement above approximately 1 W cm^{-2}. The difference between model and measurement in the lower irradiance range may be attributed to a slight overestimation of the amplitude of some of the more noisy displacement waveforms. In the automated data processing software, the amplitude was found from the difference between the maximum value after the shutter opening and the mean value of the data prior to the shutter opening. If any spikes occurred near the peak of the maximum amplitude, this could cause a slight overestimation of the amplitude. However, this factor did not appear to affect the variation in displacement with exposure duration (Fig. 8). Another plausible explanation for the difference may be the fact that the collective displacement of a portion of the pit organ is measured whereas the model uses a simple

one-dimensional geometry. The data above approximately 1 W cm^{-2} exhibit an apparent displacement limit between approximately 100 and 150 nm. This trend is once again reminiscent of the trends in the generator potential of the primary neuron (Hammer et al., 2001a). This saturation may be due to an inability of the spherule to expand beyond a certain dimension, possibly because of adjacent sensilla in the densely-packed organ.

In addition to the factors that lead to differences between model and measurement, other potential sources may contribute to the large standard deviations in Fig. 6. These include contributions due to the surface morphology and orientation of the tissue sample. Since the detection scheme depends upon backscattered light from the IR pit organ, its rough surface and orientation with respect to the optical axis are both critical. Because the beetle was aligned to the optical axis with a six-axis stage, the latter (orientation) may have a smaller contribution to the measurement error than the former (surface roughness). In addition to the degree with which the pit organ is perpendicular to the optical axis, the location from which backscattered photons originate within the depth of the organ is also important. In the current OLCR system, the longitudinal resolution is determined by the optical bandwidth ($\Delta\lambda = 60$ nm) of the source. Moreover, it is important to emphasize that due to the particular spot size of the OLCR beam, neither the displacement of a single sensillum nor that of the entire pit but the displacement from a portion of the pit (a region that contains 2–3 sensilla) is measured. Thus, there are contributions to the signal from, for example, the wax gland that accompanies each sensillum. Also, some differences in displacement may be attributed to the fact that the pit organ is composed of different tissue types with different thermal, optical, and material properties.

One final factor for consideration is the morphology of the sensillum. Although our experiments have measured only a one-dimensional displacement of all tissue layers and our simplistic model has treated the organ as a slab of bulk tissue, there is considerably more sophistication in the sensillum that may lead to complex motion. For example, the thin endocuticle layer connects adjacent sensilla but is attached to the spherule by only a thin stalk. Thus the sensilla are essentially separated from the endocuticle and each other by a cavity. The contents, if any, of the cavity and its effect on signal transduction are not known at present. The de-coupling of tissue layers can have important consequences on the motion of the organ. Whereas Fig. 9 illustrates the surface temperature rise during the exposure duration, Fig. 10 shows the temperature distribution within the tissue for several time steps during the exposure. The peak temperature in all cases occurred at the surface, although the temperature increase extended well into the depth of the tissue, beyond the depth of the spherule (vertical line). With this temperature distribution, it may be hypothesized that the cavity that surrounds the spherule may serve to isolate the responses of individual sensillum. This may impact the spatial sensitivity of the organ. Further investigation and more complex modeling are required to determine the function of all the morphological features of the pit organ.

5. Conclusion

The displacement of the IR pit organ of the beetle *Melanophila acuminata* upon absorption of infrared radiation from a helium–neon laser was measured with phase-sensitive optical low coherence reflectometry. The mean displacement at an irradiance of 1.32 W cm^{-2} was 134 nm. The displacement increased with both irradiance (energy) and exposure duration in a linear manner in close agreement with a simple one-dimensional finite difference model. This study is the first experimental investigation of the mechanism in which these unique infrared-sensitive beetles convert infrared radiation into neural signals.

Acknowledgments

The authors would like to thank Drs H. Schmitz and K.-H. Apel for their help in collecting specimen. The wood infested with beetle larvae was collected with the permission of the US Department of Agriculture–Forest Service (USDA–FS) and with considerable assistance from Terry Rogers, Entomologist, USDA–FS, Southwestern Region. Funding for this research was provided in part by grants from the Air Force Office of Scientific Research through the Multiple University Research Initiative from the Director of Defense Research and Engineering (F49620-98-1-0480), the Defense Advanced Research Projects

Agency (F49620-98-1-0489), and the Albert W. and Clemmie A. Caster Foundation.

References

Bullock, T.H., Cowles, R.B., 1952. Physiology of an infrared receptor: the facial pit of pit vipers. Science 115, 541–543.

Choi, B., Welch, A.J., 2001. Analysis of thermal relaxation during laser irradiation of tissue. Lasers Surg. Med. 29, 351–359.

Choi, B., Pearce, J.A., Welch, A.J., 2000. Modelling infrared temperature measurements: implications for laser irradiation and cryogen cooling studies. Phys. Med. Biol. 45, 541–557.

Davé, D.P., Milner, T.E., 2000. Optical low-coherence reflectometer for differential phase measurement. Opt. Lett. 25, 227–229.

Duck, F.A., 1990. Physical Properties of Tissues: A Comprehensive Reference Book. Academic Press, London.

Hammer, D.X., 2001. Infrared detection in *Melanophila acuminata.* Ph.D. thesis, University of Texas at Austin.

Hammer, D.X., Schmitz, H., Schmitz, A., Rylander III, H.G., Welch, A.J., 2001a. Sensitivity threshold and response characteristics of infrared detection in the beetle *Melanophila acuminata* (Coleoptera:Buprestidae). Comp. Biochem. Physiol. A 128, 805–819.

Hammer, D.X., Seigert, J., Stone, M.O., Rylander III, H.G., Welch, A.J., 2001b. Infrared spectral sensitivity of *Melanophila acuminata*. J. Insect Physiol. 47, 1441–1450.

Incropera, F.P., DeWitt, D.P., 1996. Fundementals of Heat and Mass Transfer. John Wiley and Sons, New York.

ISO, 1999. Lasers and laser related equipment—test methods for laser beam parameters: beam widths, divergence angle and beam propagation factor. Tech. Rep. 11146, International Standardization Organization.

Linsley, E.G., 1943. Attraction of *Melanophila* beetles by fire and smoke. J. Econ. Entomol. 36, 341–342.

Moiseenkova, V., Bell, B.A., Motamedi, M., Wozniak, E., Christensen, B.N., 2001. Wide-band spectral tuning of thermal receptors. J. Neurosci., submitted.

Pearce, J.A., Thomsen, S., 2000. Blood vessel architectural features and their effect on thermal phenomena. In: Matching the Energy Source to the Clinical Need. Society of Photo-Optical Instrumentation Engineers, Bellingham, Washington, pp. 231–277.

Querry, M.R., Wieliczka, D.M., Segelstein, D.J., 1991. Water (H_2O). In: Palik, E.D. (Ed.), Handbook of Optical Constants of Solids II. Academic Press, pp. 1059–1077.

Schmitz, H., Bleckmann, H., 1997. Fine structure and physiology of the infrared receptor of beetles of the genus *Melanophila* (Coleoptera:Buprestidae). Int. J. Insect Morphol. Embryol. 26, 205–215.

Schmitz, H., Bleckmann, H., 1998. The photomechanic infrared receptor for the detection of forest fires in the beetle *Melanophila acuminata* (Coleoptera:Buprestidae). J. Comp. Physiol. 182, 647–657.

Schmitz, H., Mürtz, M., Bleckmann, H., 2000. Responses of the infrared sensilla of *Melanophila acuminata* (Coleoptera: Buprestidae) to monochromatic infrared stimulation. J. Comp. Physiol. A 186, 543–549.

Vondran, T., Apel, K.H., Schmitz, H., 1995. The infrared receptor of *Melanophila acuminata* De Geer (Coleoptera:Buprestidae): ultrastructural study of a unique insect thermoreceptor and its possible descent from a hair mechanoreceptor. Tissue Cell 27, 645–658.